EurJIC European Journal of Inorganic Chemistry
ChemPubSoc Europe
FULL PAPER

DOI:10.1002/ejic.201500509

Dissolution of the Rare-Earth Mineral Bastnaesite by Acidic Amide Ionic Liquid for Recovery of Critical Materials

John W. Freiderich,[a] Joseph J. Stankovich,[a] Huimin Luo,[b] Sheng Dai,*[a] and Bruce A. Moyer*[a]

Keywords: Ionic liquids / Rare earths / Ion extraction / Environmental chemistry

Rare-earth elements provide the cornerstones to clean sustainable energy and modern technologies such as computers, communications, and transportation. As such, the recovery of rare earths (REs) from minerals such as bastnaesite remains important for modern times. As the light lanthanides (La–Nd) constitute the majority (typically >98.7 %) of the REs in bastnaesite with the heavy REs (Sm–Lu) contributing the remainder (approximately 1.3 %), an enrichment of heavier REs may serve as an effective means of assisting rare-earth recovery. Such an extractive metallurgy process involving ionic liquids (ILs) leads to an enrichment of heavy REs by nearly an order of magnitude. The acidic IL *N*,*N*-dimethylacetamidium bis(trifluoromethylsulfonyl)imide ($DMAH^+NTf_2^-$) in the IL 1-butyl-3-methylimidazolium bis(trifluoromethylsulfonyl)imide ($BMIM^+NTf_2^-$) dissolves froth flotation bastnaesite, synthetic bastnaesite analogues ($RECO_3F$), RE_2O_3, and $RE_2(CO_3)_3$ minerals. An overall reaction for the dissolution of bastnaesite is proposed for this IL system. This IL system may provide the initial stages of a greater RE separation scheme for bastnaesite froth flotation concentrates.

Introduction

Rare-earth elements play an important role in modern technologies including, but not limited to, high-strength magnets and energy-efficient fluorescent lighting.[1] The rare earths (REs) encompass 15 members of the 4f row (lanthanides, Z = 57–71) and a second-row transition metal, yttrium (Z = 39). All of the rare earths occur in nature except for man-made promethium (Z = 59). The lanthanides and yttrium are all thermodynamically stable trivalent ions in solution and the solid state. In addition, a phenomenon known as the lanthanide contraction is observed. This phenomenon displays an incremental decrease in the radius of the RE^{3+} ion from La^{3+} to Lu^{3+}. As a result of the stable 3+ oxidation state and the small changes in ionic radii between adjacent lanthanides, separating rare earths is challenging. In addition to lanthanides having such similar solution chemistries, the rare earths also require their ores to be processed, which has a number of industrial challenges.

The demand on industry to provide an accessible supply of these materials is ever-increasing as rare earths continue to play a more important role in applications related to modern technology. As of 2011, the majority of world rare-earth element production has occurred in China (95%), Australia (2%) and India (2.5%) contributed a little, and Brazil and Malaysia brought up the remainder (0.47%).[2,3] In China and the USA, bastnaesite is the mineral of most interest for rare-earth recovery. Bastnaesite, a rare-earth carbonate fluoride ($RECO_3F$) mineral, is approximately 7–10% rare-earth oxide (REO) consisting mostly of the lighter elements (ca. 98% La–Nd).[4]

Historically, bastnaesite has undergone a series of physicochemical processes to produce a commercial product. Considering the flow sheet for bastnaesite employed by Molycorp,[5] the following simplified process may be written:

Bastnaesite ore (7% REO) → crushing/grinding → conditioning → series of flotation steps → leaching → calciner → bastnaesite concentrate (90% REO) → separation plant

After this beneficiation process, chemical treatment of either the crude ore or the bastnaesite concentrate may take place. Kruesi and Duker of Molycorp developed one such chemical treatment process.[1,6] The process involves the bastnaesite being leached with hydrochloric acid, the resulting rare-earth fluorides [$REF_{3(s)}$] are treated with sodium hydroxide, and finally the rare-earth hydrolysis product is solubilized by hydrochloric acid again. In general, this process consists of the following steps:

$$3RECO_3F + 9HCl \rightarrow REF_3 + 2RECl_3 + 3HCl + 3H_2O + 3CO_2$$

$$REF_3 + 3NaOH \rightarrow RE(OH)_3 + 3NaF$$

$$RE(OH)_3 + 3HCl \rightarrow RECl_3 + 3H_2O$$

[a] Chemical Sciences Division,
P. O. Box 2008, Oak Ridge, TN 37831-6119, USA
E-mail: dais@ornl.gov
moyerba@ornl.gov
https://www.chem.utk.edu/faculty/sdai
[b] Energy and Transportation Science Division, Oak Ridge National Laboratory,
P. O. Box 2008, Oak Ridge, TN 37831-6119, USA

© 2015 Wiley-VCH Verlag GmbH & Co. KGaA, Weinheim

This chemical treatment process requires heating of the ore and industrial solutions to roughly 95 °C for 4 h at different stages and the consumption of 2.5 kg HCl/kg of RE_2O_3 and 0.73 kg NaOH/kg REO feed to achieve the final product.

In this work, we strived to provide an alternative to the use of aqueous solvents for the extractive metallurgy of rare earths from bastnaesite by using ionic liquids. The desirable properties of ionic liquids have been discussed extensively.[7,8] In addition, the potential application of ILs may be for the reduction/oxidation[9–12] of the RE species and/or the promotion of more stable metal–ligand complexes[13] for separation techniques. Ionic liquids have also been extensively used to dissolve metal oxides, minerals, and other compounds.[14–29]

The BASIL™ (Biphasic Acid Scavenging utilizing Ionic Liquids) process, developed by BASF, displays the green chemistry opportunities of ionic liquid applications by producing photoinitiator precursor alkoxyphenylphosphines and allowing the recycling of the IL post-process.[30] In this work, the acidic amide IL *N*,*N*-dimethylacetamidium bis(trifluoromethylsulfonyl)imide ($DMAH^+NTf_2^-$) in 1-butyl-3-methylimidazolium bis(trifluoromethylsulfonyl)imide ($BMIM^+NTF_2^-$) diluent was used to dissolve froth flotation concentrate bastnaesite and synthetic bastnaesite analogues [$RE(CO_3)F$]. To recycle the $DMAH^+NTf_2^-$ a strong mineral acid is required for reprotonation. For this process to be industrially viable more research should be conducted to develop cost-effective means of regenerating the IL. Figure 1 shows the structures of the synthesized ionic liquids.

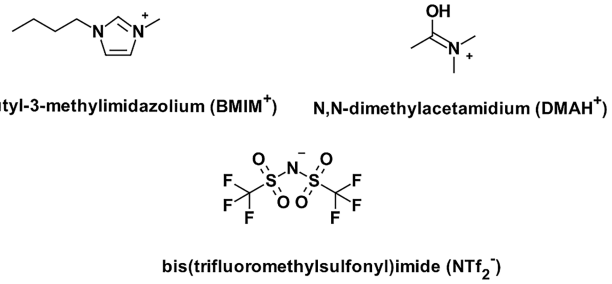

Figure 1. Structures of the synthesized ionic liquids $DMAH^+NTf_2^-$ and $BMIM^+NTF_2^-$.

Results and Discussion

Dissolution of Bastnaesite-Type Solids

A series of rare-earth carbonate fluorides ($RECO_3F$, RE = La, Ce, Pr, Nd, Eu, Tb, Dy, Ho, Y) were synthesized for use in these dissolution studies. In addition, bastnaesite analogues containing RE blends were also synthesized (see Table 1 in the Exp. Sect. for compositions). Figure 2 shows no selectivity during the dissolution process for the synthesized bastnaesite at 24 h (■). In Figure 2, the percentage of RE dissolved in the IL phase is defined by the following equation

$$\%\ \text{RE Dissolved} = \frac{[RE^{3+}]_{IL}}{[RE^{3+}]_{total}} \times 100$$

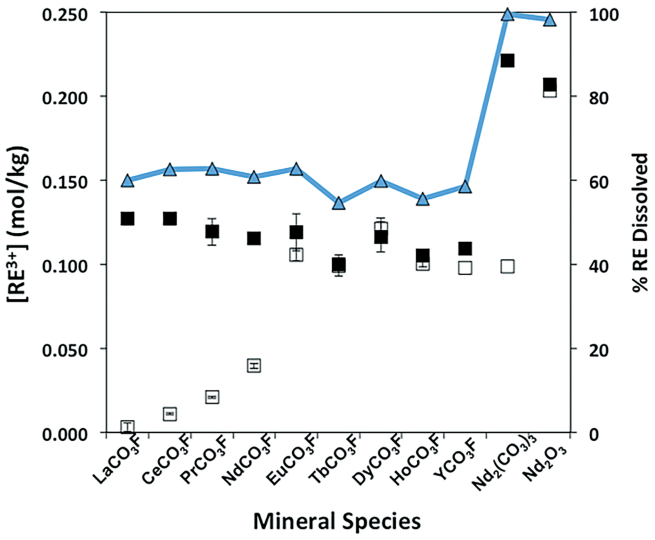

Figure 2. Dissolution of RE minerals by 2 mol/kg $DMAH^+NTf_2^-$ in $BMIM^+NTf_2^-$ at 120 °C and 1000 rpm. [RE^{3+}] shown at 1 h (□) and 24 h (■) contact times. Δ represents the % RE dissolved at 24 h. Error bars are twice the standard deviation at 95% confidence.

in which $[RE^{3+}]_{IL}$ is the concentration of the RE^{3+} metal in the IL phase, as determined through EDTA titration, and $[RE^{3+}]_{total}$ is the concentration of the RE^{3+} metal if all of the $RECO_3F$ solid could be dissolved and exist in solution. The $RECO_3F$ solids gave an average % RE Dissolved value of 60 ± 6%, which is lower than anticipated. As expected, the $Nd_2(CO_3)_3$ and Nd_2O_3 solids were quantitatively dissolved at 24 h. An unexpected result was the slow dissolution of $LaCO_3F$, $CeCO_3F$, $PrCO_3F$, and $NdCO_3F$ compared with the heavy-RE-containing $RECO_3F$ when the media was analyzed at 1 h. This led to an investigation of the structural identity of these materials.

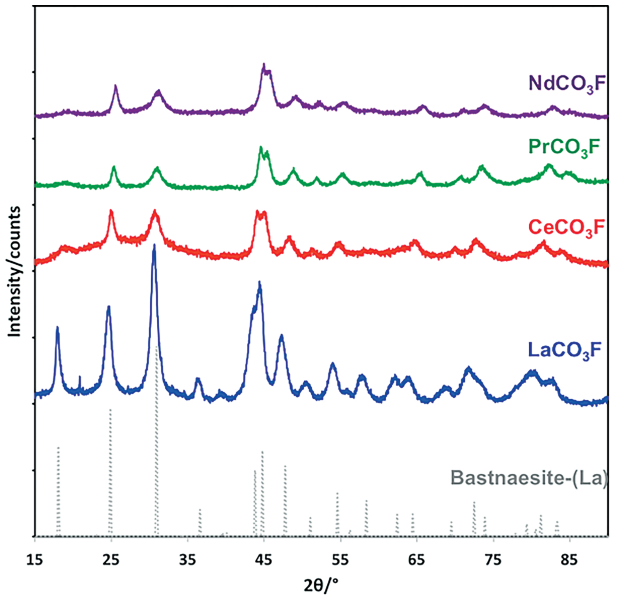

Figure 3. PXRD patterns of the synthesized $LaCO_3F$, $CeCO_3F$, $PrCO_3F$, $NdCO_3F$, and natural bastnaesite (La).

© 2015 Wiley-VCH Verlag GmbH & Co. KGaA, Weinheim

The synthesized bastnaesite analogues were characterized by using powder X-ray diffraction (PXRD). The PXRD patterns shown in Figure 3 agree well with those in the literature for $LaCO_3F$ and $CeCO_3F$.[31–33] No literature data was found for comparison with the $PrCO_3F$ or $NdCO_3F$ solids. The prepared single-$RECO_3F$ solids all appeared to crystallize as a bastnaesite-type structure with the hexagonal space group *P*62*c* for RE = La, Ce, Pr, and Nd. All four of the light lanthanides (La, Ce, Pr, Nd) show a similar diffraction pattern to that of natural bastnaesite. For the synthetic $RECO_3F$ solids with RE = Eu, Tb, Dy, Ho, and Y, the XRD patterns showed amorphous structures. Attempts to anneal these heavier RE solids, so a recognizable XRD pattern could be collected, yielded a black powder. The PXRD pattern of the black powder did not match that of $RECO_3F$ and is believed to be REOF.

Because the PXRD patterns of the heavier RE solids showed amorphous structures, FTIR-ATR spectroscopy was used to qualitatively determine the coordination of the CO_3^{2-} anion in the $RECO_3F$ matrix. Figure 4a displays the IR spectra of a series of synthesized bastnaesite analogues containing single rare earths and blends of rare earths and Figure 4b allows comparison of the spectra of the heavier $TbCO_3F$ and YCO_3F with those of $Tb_2(CO_3)_3$ and $Y_2(CO_3)_3$. Although the heavy-$RECO_3F$ solids do not appear to be explicitly "bastnaesite-like", it can be stated that they are not RE carbonates either. A clear change in the light- and heavy-$RECO_3F$ synthetic minerals occurs between Nd and Tb. The amorphous nature of the heavy-RE minerals coupled with the change in CO stretching at around 1500 cm^{-1} between $NdCO_3F$ and $TbCO_3F$ indicates a change in the overall structure of the bastnaesite analogues.

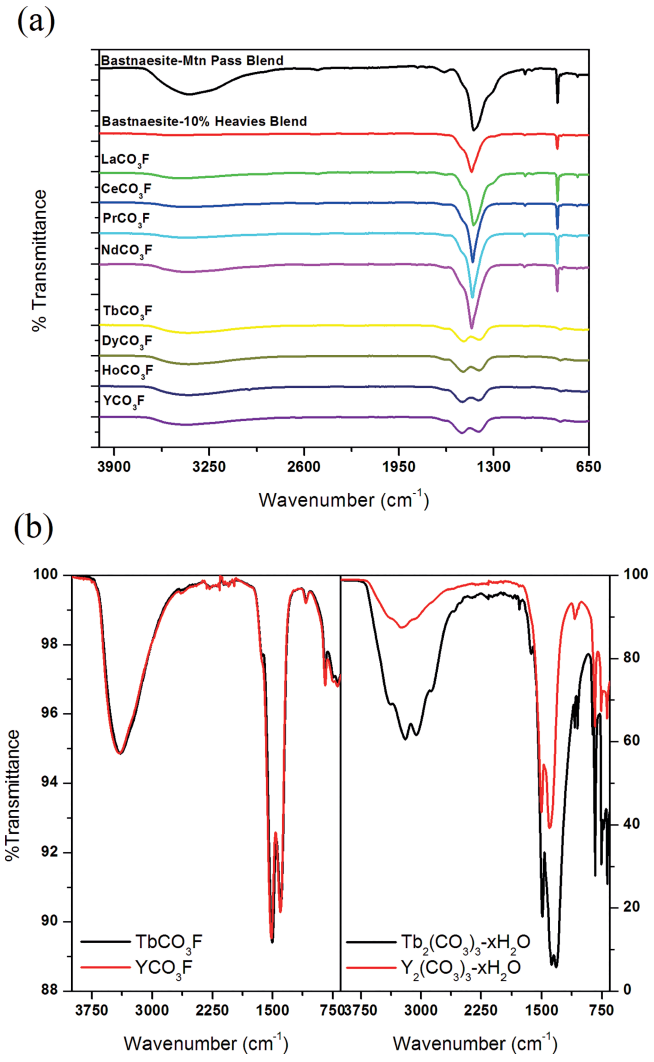

Figure 4. (a) FTIR-ATR spectra of synthetic bastnaesite and $RECO_3F$ solids. (b) Comparison of the FTIR-ATR spectra of $RECO_3F$ with $RE_2(CO_3)_3$ solids.

Role of Carbonate Chemistry in Dissolution

The dissolution of $Nd_2(CO_3)_3$ was significantly slower than that of Nd_2O_3 and the contrast between the dissolution of carbonate and oxide species assists in providing a further understanding of the chemistry responsible for the dissolution of the bastnaesite structure in $BMIM^+NTf_2^-$.

As the dissolution of the $Nd_2(CO_3)_3$ and Nd_2O_3 progresses at seemingly different rates, this raised the question of the role of CO_3^{2-} in the interaction of $DMAH^+$ with $RECO_3F$. To further understand the role of CO_3^{2-} in these systems, two tests were carried out on $HoCO_3F$, which had already been shown to have a faster dissolution within 1 h. The first test was to run the same experiment under the same conditions, but instead cap the vial and create a closed system. The second test was to flush a stream of $CO_{2(g)}$ over the IL solution as the reaction proceeded. In both cases the dissolution reaction was suppressed and only 8.2 ± 0.4% of the $HoCO_3F$ dissolved within 1 h instead of the 53 ± 5% (Figure 2) that dissolved in the open system. This appears to be in agreement with the observation of gas evolution through the IL; chemical intuition hints that this is most likely $CO_{2(g)}$. So, the Nd_2O_3 is dissolved by the $DMAH^+NTf_2^-$ according to the following reaction:

$$Nd_2O_3 + 6DMAH^+NTf_2^- \rightarrow 2Nd(DMA)_3(NTf_2)_3 + 3H_2O$$

whereas, most likely, $Nd_2(CO_3)_3$ is dissolved in two reactions:

$$Nd_2(CO_3)_3 + 6DMAH^+NTf_2^- \rightarrow 2Nd(DMA)_3(NTf_2)_3 + 3H_2CO_3$$

$$3H_2CO_3 \rightarrow 3CO_{2(g)} + 3H_2O$$

As a result of carbonic acid disproportionation in the IL, it seems that this reaction slows down the dissolution process as the system waits to expel $CO_{2(g)}$.

Rare-Earth Fluoride Precipitation

After each $RECO_3F$ dissolution experiment, solid remained in the bottom of each vial. This solid was analyzed by PXRD and determined to be $REF_{3(s)}$ (Figure 5). This result was not all that surprising as dissolution of the RE^{3+} into solution would presumably liberate F^- from the

 © 2015 Wiley-VCH Verlag GmbH & Co. KGaA, Weinheim

bastnaesite. A light (Nd) and heavy (Ho) $RECO_3F$ were chosen for analysis, post-dissolution.

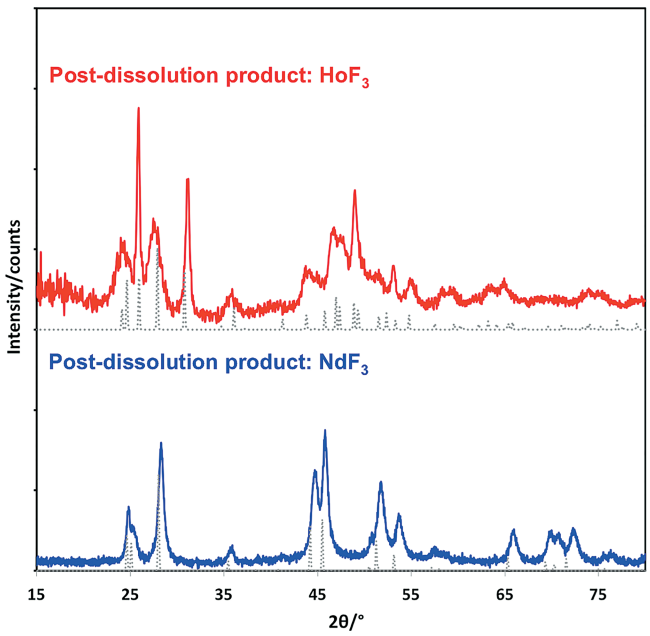

Figure 5. PXRD patterns of $NdCO_3F$ post-dissolution as NdF_3 (blue) and $HoCO_3F$ post-dissolution as HoF_3 (red) after 5 h. Literature powder patterns for NdF_3 and HoF_3 are shown for comparison.

In addition to the formation of REF_3 post-dissolution, the RE^{3+} in the IL phase was also analyzed for varying total amounts of $RECO_3F$. The number of mmol of RE^{3+} in the IL phase was plotted versus the total number of mmol of $RECO_3F_{(s)}$ in the system (Figure 6) and yielded slopes of 0.61 ± 0.06, 0.58 ± 0.04, and 0.57 ± 0.07 for Nd, Dy, and Ho, respectively, which shows that roughly 2/3 of the RE exists in the IL phase after dissolution. The observation of $REF_{3(s)}$ coupled with the slope analysis for one light (Nd) and two heavy (Dy, Ho) REs suggests that the chemistry of dissolution of $RECO_3F$ is similar across the rare-earth series.

Having established the above information, the following points can be concluded:

1) Gas evolves as a result of $DMAH^+NTf_2^-$ contact with $RECO_3F$, $Nd_2(CO_3)_3$, and Nd_2O_3.

2) An open system allows the dissolution process to proceed whereas a closed system or a system flushed with $CO_{2(g)}$ suppresses the dissolution of $RECO_3F$.

3) The PXRD pattern of the resulting RE solid after $RECO_3F$ is dissolved by $DMAH^+NTf_2^-$ indicates that REF_3 is a product of dissolution.

4) Only 2/3 of the RE^{3+} in the system post-dissolution exists in the IL phase. The other 1/3 exists as REF_3 solid.

5) Acid dissociation constants in aqueous media (μ = 0.0 M, 25 °C) for HF (pK_a = 3.17) and H_2CO_3 ($pK_{a,1}$ = 6.35, $pK_{a,2}$ = 10.34)[34] suggest that carbonic acid forms preferentially to hydrofluoric acid.

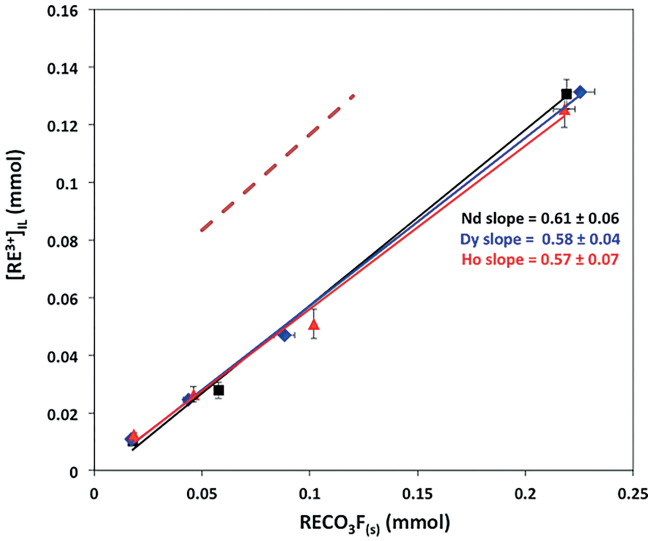

Figure 6. Dissolution of $NdCO_3F$ (black filled square), $DyCO_3F$ (blue filled diamond), and $HoCO_3F$ (red triangle) for varying total amounts of $RECO_3F$ in a system in contact with 2 mol/kg $DMAH^+NTf_2^-$ in $BMIM^+NTf_2^-$ at 120 °C and 1000 rpm for 5 h. A dashed line with a slope of 2/3 is provided for comparison.

From these considerations, the reaction scheme shown in Figure 7 is likely. The surface of the $RECO_3F$ reacts with the H^+ of $DMAH^+$ to form soluble $RE(DMA)_2(NTf_2)_2F$ and carbonic acid (H_2CO_3). These two species react by two different pathways. $RE(DMA)_2(NTf_2)_2F$ reacts with other $RE(DMA)_2(NTf_2)_2F$ to form soluble $RE(DMA)_2(NTf_2)_3$ and insoluble REF_3, and H_2CO_3 produces carbon dioxide gas and water, both of which leave the IL at 120 °C. Although there remains unconsumed H^+ in the IL phase, in the form of $DMAH^+NTf_2^-$ (pK_a = –0.19 at 25 °C in sulfuric acid),[35] it seems that the remainder of H^+ does not compete with RE^{3+} for F^- and $REF_{3(s)}$ precipitates

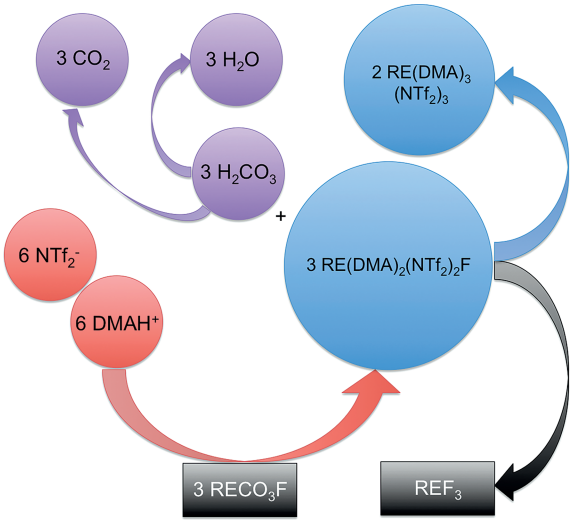

Figure 7. Proposed reaction scheme for the dissolution process in the IL system. Red circles indicate initial reactive solution species, black rectangles indicate solid phases, purple circles indicate species that exist in the system as gases, and blue circles indicate RE solution species.

© 2015 Wiley-VCH Verlag GmbH & Co. KGaA, Weinheim

out of solution as a result. The following dissolution reactions are proposed:

$3RECO_3F_{(s)} + 6DMAH^+NTf_2^- \rightarrow 3RE(DMA)_2(NTf_2)_2F + 3H_2CO_3$

$3RE(DMA)_2(NTf_2)_2F \rightarrow REF_{3(s)} + 2RE(DMA)_3(NTf_2)_3$

$3H_2CO_3 \rightarrow 3CO_{2(g)} + 3H_2O$

$3RECO_3F_{(s)} + 6DMAH^+NTf_2^- \rightarrow 2RE(DMA)_3(NTf_2)_3 + REF_{3(s)} + 3CO_{2(g)} + 3H_2O$

Solution Chemistry of Nd^{3+} in $BMIM^+NTf_2^-$

As the $RECO_3F$ mineral is dissolved by $DMAH^+NTf_2^-$, the RE^{3+} species that is liberated from the solid phase becomes solvated by the constituents of the IL phase. In this system, DMA, $DMAH^+NTf_2^-$, and $BMIM^+NTf_2^-$ are present in sufficient concentrations to accomplish the task of RE^{3+} solvation. The following equilibrium was considered for ascertaining Nd^{3+} speciation in $BMIM^+NTf_2^-$:

$Nd^{3+} + n\text{DMA} \rightleftarrows Nd(DMA)_n^{3+}$ (n = 1–5)

The final Nd^{3+}/DMA species was found to be a 1:5 complex in $BMIM^+NTf>_2^-$ at 120 °C as no further spectral features evolved as a result of increasing the Nd^{3+}/DMA ratio beyond 1:7. The best-fit stability constants for these Nd^{3+}/DMA complexes were determined to be $\log\beta_{101}$ = 2.12 ± 0.05, $\log\beta_{102}$ = 6.72 ± 0.05, $\log\beta_{103}$ = 8.76 ± 0.05, $\log\beta_{104}$ = 10.72 ± 0.05, and $\log\beta_{105}$ = 9.70 ± 0.05. Figure 8 shows the hypersensitive $^4F_{5/2}$, $^2H_{9/2} \leftarrow {}^4I_{9/2}$ transition[36] of the Nd^{3+} ion and the speciation of the metal as it is complexed at increasing concentration of *N*,*N*-dimethylacetamide, the conjugate base of the acidic ionic liquid $DMAH^+NTf_2^-$. For the dissolution process under the experimental conditions stated earlier, the average number of ligands n bound to Nd^{3+} is 2.91; however, this does not account for the number of potential DMA ligands that may bind with Nd^{3+} as a result of partially dissociated $DMAH^+$, so the number may be greater.

In addition to the DMA titration of Nd^{3+}, $DMAH^+NTf_2^-$ and $HNTf_2$ were also used as titrants. $HNTf_2$ showed no interaction with Nd^{3+}, whereas $DMAH^+NTf_2^-$ showed some interaction with Nd^{3+} through minor changes in the spectral features of Nd^{3+}, but no fit could be made of the data. However, it is not clear whether the $DMAH^+$ ion interacts with Nd^{3+} to form the $Nd(DMAH)^{4+}$ complex or the acid dissociates to a reasonable extent allowing for Nd^{3+} and DMA to interact. If any mode of interaction occurs, it is most likely the latter.

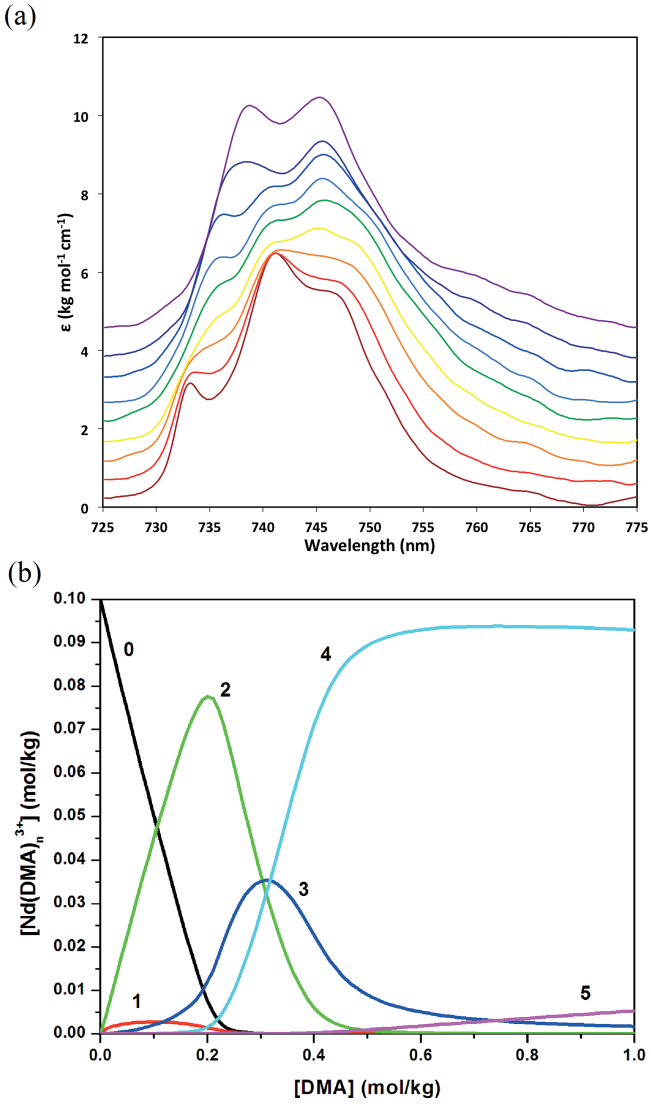

Figure 8. (a) Absorbance spectra and (b) speciation of Nd^{3+} in $BMIM^+NTf_2^-$ at 120 °C. The following species are present: 0: Nd^{3+}; 1: $Nd(DMA)^{3+}$; 2: $Nd(DMA)_2^{3+}$; 3: $Nd(DMA)_3^{3+}$; 4: $Nd(DMA)_4^{3+}$; 5: $Nd(DMA)_5^{3+}$. Experimental Nd^{3+}/DMA ratios range from 1:0 to 1:7.25. Note: The Nd spectra are shifted in order to display the features of each.

Dissolution of Bastnaesite and Synthetic Bastnaesite RE Blends

The surprising result of a seemingly kinetically limited dissolution of light-$RECO_3F$ compared with heavy-$RECO_3F$ (Figure 2) prompted an exploration of the dissolution process of natural bastnaesite. A froth flotation bastnaesite product (enriched in RE) was provided by Molycorp and two bastnaesite solids were synthesized as well. The compositions of these synthesized materials are presented in Table 1 in the Exp. Sect. The dissolution behavior of the synthesized bastnaesite materials containing the entire range of RE was not particularly intriguing as these solids dissolved in nearly the same ratios as their chemical make-up.

As was observed with the single-RE bastnaesite solids, the heavy REs in natural bastnaesite also dissolved more quickly than the light REs. To observe this phenomenon the temperature of the system was lowered to 45 °C with a stirring rate of 700 rpm. The ratio of the total amount of heavy- to light-REs was calculated to determine the enrichment effect over time. The [RE] in the IL was determined by ion chromatography (IC). Each RE was calibrated by IC to be in the range 50 ppb–1 ppm by using the following expression

 © 2015 Wiley-VCH Verlag GmbH & Co. KGaA, Weinheim

$$\text{Fraction}\ \frac{\text{Heavy}}{\text{Light}} = \frac{\Sigma_{\text{Lu}}{}^{\text{Sm}}[\text{RE}]_i}{\Sigma_{\text{Nd}}{}^{\text{La}}[\text{RE}]_i}$$

in which $\Sigma_{\text{Lu}}^{\text{Sm}}[\text{RE}]_i$ is the contribution to the total heavy-rare-earth concentration in the IL phase for RE = Sm, Eu, Gd, Tb, Dy, Ho, Er, Tm, Yb, Lu, and Y, and $\Sigma_{\text{Nd}}^{\text{La}}[\text{RE}]_i$ is the contribution to the total light-rare-earth concentration in the IL phase for RE = La, Ce, Pr, and Nd. Figure 9 shows the enrichment as a function of time. Although enrichment of the heavy REs may occur near the beginning of the dissolution process, over the course of time it appears that a combination of events may occur such that the enrichment then decreases again. These events are 1) the kinetically limited dissolution of the light REs finally catching up the dissolution of the heavy REs and 2) the formation of REF_3 as a result of F^- being liberated into the IL.

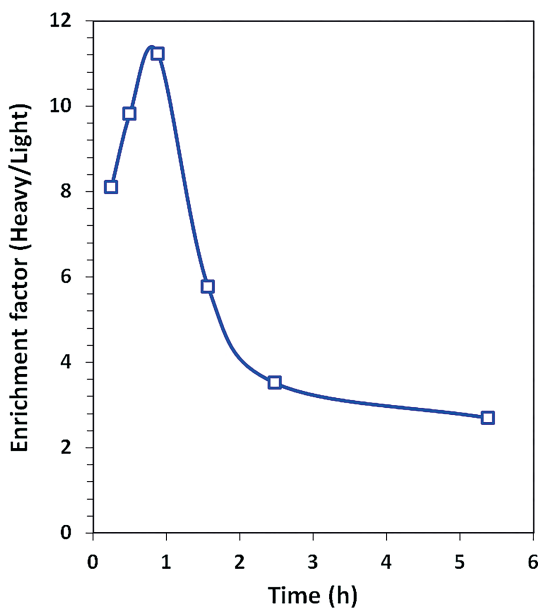

Figure 9. Enrichment factor [quotient (□) of the heavy to light ratio in 2 mol/kg $DMAH^+NTf_2^-$ in $BMIM^+NTf_2^-$ divided by the ratio of heavy to light REs in natural bastnaesite] as a function of time. Conditions: 45 °C and 700 rpm.

Although the enrichment of the heavy REs (Figure 9) occurs up to around 1 h, after this time the ratio of heavy REs to light REs decreases quickly. The enrichment factor changes throughout the dissolution process. This may be a result of the light REs (La–Nd) finally starting to have a greater uptake in the IL diluent. Increasing the scale of the dissolution experiment by a factor of 60 yielded a higher enrichment factor (0.37 heavy/light) than found on the smaller scale. This factor was achieved after 15 min of the ore being in contact with the heated ionic liquid. Figure 10 shows the fraction of heavy/light rare earths in the stripped samples as time progresses. Over the course of 4 h there was no substantial increase in the concentration of the rare earths in the samples; after 4 h there was a 23% increase in the concentration of the light rare earths and virtually no increase in the concentration of the heavy rare earths.

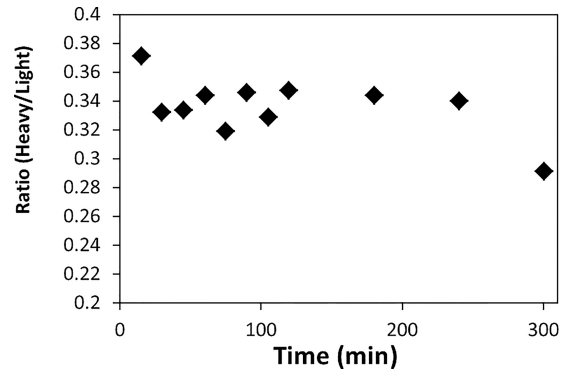

Figure 10. Ratio of heavy/light rare earths in 2 mol/kg $DMAH^+NTf_2^-$ in $BMIM^+NTf_2^-$ diluent as natural bastnaesite is dissolved as a function of time. Bastinite (3 g) was dissolved in 62.3 g of IL. Conditions: 45 °C and 700 rpm.

This set of experiments was motivated by the froth flotation ore likely not being homogeneous and that increasing the size of the starting sample would make consistency less of a concern. The results demonstrate that froth flotation bastnaesite is likely not homogeneous, also that upscaling the process seems to affect the kinetics. The same weight ratio of naturally occurring bastnaesite ore to IL was used for both the small- and large-scale experiments. It is possible for this ionic liquid system to be used with other rare-earth minerals and gangue minerals.

Conclusions

The dissolution process of bastnaesite-type solids in an ionic liquid system has been demonstrated. The $RECO_3F$ bastnaesite mineral was shown to consume two acidic protons during the dissolution process and to form both soluble RE^{3+} and insoluble REF_3. The heavy REs (Eu–Ho, Y) dissolve faster than the light REs (La–Nd) in this IL system, regardless of whether the materials are single-$RECO_3F$ or natural bastnaesite, and the process allows heavy-RE enrichment in the IL for a period of time. Although an IL system has densely concentrated ions and shows potential solvation capability and ionic interactions with the RE^{3+} ions, the precipitation of REF_3 was not suppressed. In addition, the liberation of CO_2 from the dissolution process is necessary to push the reaction forward. The overall dissolution reaction proposed for this IL system is as follows: $3RECO_3F_{(s)} + 6DMAH^+NTf_2^- \rightarrow 2RE(DMA)_3(NTf_2)_3 + REF_{3(s)} + 3CO_{2(g)} + 3H_2O$. This work illustrates one of the first uses of a purely ionic liquid system to dissolve rare-earth minerals.

Experimental Section

***N,N*-Dimethylacetamidium Bis(trifluoromethylsulfonyl)imide ($DMAH^+NTf_2^-$) Ionic Liquid:** Batches of this ionic liquid were synthesized by combining the neutralization and metathesis methodologies previously described by Luo et al.[37] At room temperature, *N,N*-dimethylacetamide (4.03 g, 0.046 mol) was mixed with a slight

 © 2015 Wiley-VCH Verlag GmbH & Co. KGaA, Weinheim

excess of concentrated aqueous HCl. $LiNTf_2$ dissolved in deionized water was added in an equal molar ratio to this mixture. After stirring, two phase were present with water on the top and $DMAH^+NTf_2^-$ on the bottom. The IL layer was separated from the water and washed several times with deionized water to remove any LiCl still in the IL. The resulting nearly colorless liquid was dried under vacuum at 70 °C for 4 h and characterized by thermogravimetric analysis and NMR spectroscopy, yield 94%. ^{1}H NMR (400.13 MHz, $CDCl_3$): δ = 8.07 (br., 1 H), 3.33 (s, 3 H), 3.26 (s, 3 H), 2.48 (s, 3 H) ppm. ^{13}C NMR (100.61 MHz, $CDCl_3$): δ = 174.45 (C), 119.57 (q, $J_{C,F}$ = 320.1 Hz, CF_3), 39.69 (CH_3), 37.68 (CH_3), 17.84 (CH_3) ppm.

1-Butyl-3-methylimidazolium Bis(trifluoromethylsulfonyl)imide ($BMIM^+NTf_2^-$) Ionic Liquid: $BMIM^+NTf_2^-$ was synthesized according to a modified procedure reported in the literature.[38] Methylimidazole (20.0 g, 243.0 mmol) was allowed to react with 1-bromobutane (34.0 g, 312.0 mmol) in dry THF under nitrogen. The mixture was stirred vigorously at room temperature for 24 h and the resulting white precipitate was isolated and washed repeatedly with ethyl acetate (3 × 100 mL) to remove any unreacted starting materials. The resulting $BMIM^+Br^-$ salt was dried under vacuum (yield: 90%). This $BMIM^+Br^-$ salt (20.0 g, 105.0 mmol) was mixed with $LiNTf_2$ (45.0 g, 156.8 mmol) in water (20 mL) and the mixture stirred overnight to obtain $BMIM^+NTf_2^-$ as a colorless liquid. The ionic liquid was dried in vacuo at 333 K for 24 h. ^{1}H NMR (400 MHz, [D_6]DMSO): δ = 9.10 (s, 1 H), 7.75 (s, 1 H), 7.67 (s, 1 H), 4.19 (q, J = 7.2 Hz, 2 H), 3.85 (s, 3 H), 1.42 (t, J = 7.2 Hz, 3 H) ppm.

Synthesis of Rare-Earth Bastnaesite Analogues: Bastnaesite analogues containing a single lanthanide or yttrium were synthesized following the literature procedure of Janka and Schleid.[31] $(Y,Ln)(NO_3)_3{\cdot}xH_2O$ solid (15 mmol) was dissolved in H_2O (250 mL) and the mixture was continuously stirred. A solution containing NaF (13 mmol) and $NaHCO_3$ (13 mmol) in H_2O (500 mL) was added slowly to this $Ln(NO_3)_3$ solution over 6 h. The resulting solid and supernatant were then stirred for 30 min, filtered through 0.2 µm Millipore filters and washed with 18 M H_2O (3 × 100 mL) to remove remaining $NaNO_3$ and unreacted $Ln(NO_3)_3$, NaF, and $NaHCO_3$. The resulting powder was collected and dried in an oven at 120 °C.

A slight modification to synthesize bastnaesite analogues containing multiple REs was accomplished by blending the $RE(NO_3)_3{\cdot}xH_2O$ solids pre-synthesis. Table 1 shows the distributions of the REs in each material.

Neodymium Bis(trifluoromethylsulfonyl)imide [$Nd(NTf_2)_3$]: $Nd(NTf_2)_3$ solid was prepared according to the reaction $Nd_2O_3 + 6HNTf_2 \rightarrow 2Nd(NTf_2)_3 + 3H_2O$. Nd_2O_3 (5.2 mmol, 1.74 g) was suspended by stirring in deionized water (5 mL) at 20 °C as 80% $HNTf_2$ (10.9 g) was added to the solution. When no Nd_2O_3 remained, the solution was heated to 120 °C under a blanket of Ar to drive off excess $HNTf_2$ and water. The resulting slightly-purple solid was titrated to determine the Nd^{3+} content and identified to be $Nd(NTf_2)_3{\cdot}2H_2O$. This solid was stored under Ar for later use.

X-ray Diffraction Analysis: Continuous θ–2θ scans were performed with a PANalytical Empyrean diffractometer equipped with a Pixcel 3D detector from nominally 15 to 90° 2θ in 10 min using Cu-K_α radiation (l = 1.5405981 Å) and the X'Celerator detector. All the scans used 1/2° fixed slits and 1° anti-scatter slits. A search match was conducted by using the "Jade" and/or HighScore software and the International Center for Diffraction Data (ICDD) database. "HighScore Plus".[44]

Table 1. Composition of synthetic bastnaesite analogues.

Rare-earth element	Bastnaesite – mountain pass blend [%][a]	Bastnaesite/10% heavies blend enriched [%]
La	33.8	17.2
Ce	49.6	34.4
Pr	4.1	5.2
Nd	11.2	17.2
Sm	0.9	4.3
Eu	0.1	4.3
Gd	0.2	3.0
Tb	0	0.5
Dy	0	3.0
Ho	0	0.7
Er	0	2.2
Tm	0	0.3
Yb	0	1.5
Lu	trace	0.3
Y	0.1	5.7

[a] Percentages based on the 2010 USGS Investigation Report.[43]

FTIR-ATR Spectroscopy: FTIR-ATR spectra were collected with a Perkin Elmer Frontier FTIR spectrometer equipped with a diamond ATR. Scans were performed in the range 4000–650 cm^{-1} at a resolution of 4 cm^{-1}. The crystal was cleaned in between runs with 2-propanol.

Rare-Earth Dissolution: A 2 mol/kg $DMAH^+NTf_2^-$ solution in $BMIM^+NTf_2^-$ was used to dissolve the bastnaesite analogues $Nd_2(CO_3)_3$ and Nd_2O_3. For each replicate, a 10-fold excess of acid to RE was used to ensure completion of the reaction. This typically involved the contact of RE solid (0.2 mmol) with IL solution (1 g) in 4 mL boroscilicate glass vials. The IL solution was heated to 120 °C prior to contact with the RE solids and the suspended solids were mixed at around 1000 rpm for 1 or 24 h, exposed to the atmosphere. After the contact time, these samples were centrifuged at 3000 rpm for 40 min to ensure complete separation of remaining solid from the IL.

To assess the kinetics of the system on the froth flotation of bastnaesite, the temperature was set to 45 °C with stirring at 700 rpm. Aliquots of 30 µL were taken and quenched in dichloroethane (DCE). This DCE phase was then contacted with a 2% HNO_3 phase in a 1:1 volume ratio and agitated for 10 min. Under these system conditions, the RE was stripped into the aqueous phase at >99% and the IL remained behind in the DCE phase. These prepared nitric acid phases were injected into the IC.

To examine the kinetics of a larger scale version of this system, bastnaesite (3 g) was dissolved in a 10-fold excess of 2 mol/kg $DMAH^+NTf_2^-$ in $BMIM^+NTf_2^-$ solution (62.3 g) at a temperature of 45 °C with stirring at 1000 rpm. Aliquots of 100 µL were taken and quenched in DCE and stripped by using 2% HNO_3. The stripped solutions were diluted appropriately and investigated by inductively coupled plasma mass spectrometry (ICP-MS; Thermo Scientific Xseries 2 Q-ICP-MS).

Determination of the Rare Earth Concentration

EDTA–Ln Titrations: The resulting IL phases were titrated according to previous literature on spectrophotometric RE determinations in aqueous media.[39–41] Small aliquots (10–20 µL) of the RE-containing IL phase were dissolved in 0.1 mol/L sodium acetate buffer (5 mL; pH 5). These solutions were spiked with Xylenol Orange in distilled water. A 0.01 mol/L Na_2EDTA solution was used to titrate the RE acetate solution. The solutions changed from red to yellow to indicate that all the RE^{3+} in solution had been complexed by EDTA.

 © 2015 Wiley-VCH Verlag GmbH & Co. KGaA, Weinheim

Ion Chromatography: To analyze several lanthanides simultaneously, a DIONEX DX-500 Ion Chromatograph with an AD20 Absorbance Detector and Pneumatic Postcolumn controller was used. An IonPac CG5A Guard (P/N 046104) and CS5A Analytical Column (P/N 046100) were used with the following eluent mixture: 63% 160 mM oxalic acid/100 mM potassium hydroxide/200 mM tetramethylammonium hydroxide, 4% 160 mM diglycolic acid/190 mM potassium hydroxide, and 33% degassed deionized water. The flow rate was set to 1.2 mL/min with a back pressure of 1750 psi. The post column reagent used was 0.5 mM 4-(2-pyridylazo)resorcinol (PAR, P/N 39672 in Met Pac PAR) postcolumn reagent diluent (P/N 046094). Injections of 2% nitric acid containing RE/IL aliquots allowed for baseline resolution of RE peaks (except Pr and Nd) in the chromatograms and linearity of the signal response from 50 ppb to 1 ppm.

Inductively Coupled Plasma Mass Spectrometry: Six-point calibration curves for all the rare earths were prepared for concentrations in the range 0.1–100 ppb with correlation coefficients >0.999. An indium internal standard at 6 ppb was used in conjunction with a 2% nitric acid carrier for all samples. The instrument software was used to determine the concentrations when the dilution factors were input into the system. Dilution factors for all samples were 8000.

Spectrophotometric Titrations: The absorption spectra of $Nd(NTf_2)_3$ in $BMIM^+NTf_2^-$ were collected with a 1 cm pathlength over the wavelength range 500–900 nm with a USB4000-VIS-NIR spectrophotometer (Ocean Optics, Dunedin, FL, USA) equipped with a tungsten-halogen source and an Ocean Optics TP300-UV/Vis Transmission Dip Probe. A 0.09 mol/kg $Nd(NTf_2)_3$ solution in $BMIM^+NTf_2^-$ was titrated with 6 mol/kg *N*,*N*-dimethylacetamide in $BMIM^+NTf_2^-$ at 120 °C. The stability constants for the Nd^{3+}/*N*,*N*-dimethylacetamide complexes were calculated by nonlinear least-square regression in HypSpec.[42]

Acknowledgments

The authors thank Dr. Dale Ensor (Tennessee Technological University) and Dr. Colt Heathman (CSD) for useful solution chemistry discussions as well as Dr. Richard Mayes (CSD) of ORNL regarding XRD. Research funded by the Critical Materials Institute, an Energy Innovation Hub funded by the U.S. Department of Energy, Office of Energy Efficiency and Renewable Energy, Advanced Manufacturing Office.

[1] C. K. Gupta, N. N. Krishnamurthy, *Extractive Metallurgy of Rare Earths*, CRC Press, Washington, DC, **2005**.
[2] K. A. Gschneidner Jr., *Mater. Matters (Aldrich)* **2011**, *6*, 32–37.
[3] M. Humphries, *Rare Earth Elements*, The Global Supply Chain, Congressional Research Service, **2013**, content downloaded from https://www.fas.org/sgp/crs/natsec/R41347.pdf on 8/12/2015.
[4] J. B. Hedrick, "Rare Earths", in *Metals and Minerals*, U.S. Geological Survey Minerals Yearbook **2001**, vol. *I*, 61.1–61.17.
[5] F. F. Aplan, *The processing of rare-earth minerals. The Minerals*, Metals and Materials Society, Warrendale, PA, USA, **1988**.
[6] P. R. Kruesi, G. Duker, *Min. Met. Mater. S* **1965**, *17*, 847.
[7] K. Binnemans, *Chem. Rev.* **2007**, *107*, 2592–2614.
[8] T. Welton, *Chem. Rev.* **1999**, *99*, 2071–2083.
[9] a) A. Kurachi, M. Matsumiya, K. Tsunashima, S. Kodama, *J. Appl. Electrochem.* **2012**, *42*, 961–968.
[10] Y. F. Pan, C. L. Hussey, *Inorg. Chem.* **2013**, *52*, 3241–3252.
[11] A. I. Bhatt, I. May, V. A. Volkovich, D. Collison, M. Helliwell, I. B. Polovov, R. G. Lewin, *Inorg. Chem.* **2005**, *44*, 4934–4940.
[12] L. H. Chou, W. E. Cleland, C. L. Hussey, *Inorg. Chem.* **2012**, *51*, 11450–11457.
[13] L. S. Liu, G. X. Tian, L. F. Rao, *Solvent Extr. Ion Exch.* **2013**, *31*, 384–400.
[14] J. A. Whitehead, G. A. Lawrance, A. McCluskey, *Green Chem.* **2004**, *6*, 313–315.
[15] S. Wellens, T. V. Hoogerstraete, C. Möller, B. Thijs, J. Luyten, K. Binnemans, *Hydrometallurgy* **2014**, *144*, 27–33.
[16] A. Kilicarslan, M. N. Saridede, S. Stopic, B. Friedrich, *Int. J. Min. Met. Mater.* **2014**, *21*, 138–143.
[17] A. P. Abbott, G. Frisch, J. Hartley, K. S. Ryder, *Green Chem.* **2011**, *13*, 471–481.
[18] T. Dong, Y. Hua, Q. Zhang, D. Zhou, *Hydrometallurgy* **2009**, *1–2*, 33–38.
[19] J. A. Whitehead, J. Zhang, A. McCluskey, G. A. Lawrance, *Hydrometallurgy* **2009**, *3–4*, 276–280.
[20] J. Luczak, M. Joskowska, J. Hupka, *Physicochem. Probl. Mi.* **2008**, *42*, 223–236.
[21] J. A. Whitehead, J. Zhang, N. Pereira, A. McCluskey, G. A. Lawrance, *Hydrometallurgy* **2007**, *88*, 109–120.
[22] A. P. Abbott, G. Capper, D. L. Davies, R. K. Rasheed, P. Shikotra, *Inorg. Chem.* **2005**, *44*, 6497–6499.
[23] P. Nockemann, B. Thijs, S. Pittois, J. Thoen, C. Glorieux, K. Van Hecke, L. Van Meervelt, B. Kirchner, K. Binnemans, *J. Phys. Chem. B* **2006**, *110*, 20978–20992.
[24] D. Dupont, K. Binnemans, *Green Chem.* **2015**, *17*, 2150–2163.
[25] D. Dupont, K. Binnemans, *Green Chem.* **2015**, *17*, 856–868.
[26] I. Billard, C. Gaillard, C. Henniq, *Dalton Trans.* **2007**, *37*, 4214–4221.
[27] S. Wellens, N. R. Brooks, B. Thijs, L. Van Meervelt, K. Binnemans, *Dalton Trans.* **2014**, *43*, 3443–3452.
[28] A. Yao, T. Chu, *Dalton Trans.* **2013**, *42*, 8413–8419.
[29] C. M. Wai, Y. J. Laio, W. Laio, G. Tian, R. S. Addleman, D. Quach, S. P. Pasilis, *Dalton Trans.* **2011**, *40*, 5039–5045.
[30] N. V. Plechkova, K. R. Seddon, *Chem. Soc. Rev.* **2008**, *37*, 123–150.
[31] O. Janka, T. Schleid, *Eur. J. Inorg. Chem.* **2009**, 357–362.
[32] I. Oftedal, *Z. Kristallogr. Kristallgeom. Kristallphys. Kristallchem.* **1930**, *72*, 239–248.
[33] Y. Shaohua, L. Yao, Z. Fengyun, W. Wenyuan, *Trans. Nonferrous Met. Soc. China* **2011**, *21*, 2306–2310.
[34] R. M. Smith, A. E. Martell, *Critical Stability Constants,* Plenum Press, New York, **1974**.
[35] J. A. Riddick, W. B. Bunger, T. K. Sakano, *Techniques of Chemistry*, 4th ed., volume II, *Organic Solvents*, Wiley, New York, **1985**.
[36] D. G. Karraker, *Inorg. Chem.* **1968**, *7*, 473.
[37] H. M. Luo, J. F. Huang, S. Dai, *Sep. Sci. Technol.* **2010**, *45*, 1679–1688.
[38] P. Bonhote, A. P. Dias, N. Papageorgiou, K. Kalyanasundaram, M. Gratzel, *Inorg. Chem.* **1996**, *35*, 1168–1178.
[39] M. A. E. Hafez, A. M. A. Abdallah, N. E. A. Elgany, *Analyst* **1990**, *115*, 221–224.
[40] K. Tonosaki, M. Otomo, *Chem. Soc. Jpn.* **1962**, *35*, 1683–1686.
[41] K. N. Munshi, A. K. Dey, *Anal. Chem.* **1964**, *36*, 2003.
[42] P. Gans, A. Sabatini, A. Vacca, *Talanta* **1996**, *43*, 1739–1753.
[43] Downloaded from: http://pubs.usgs.gov/sir/2010/5220/downloads/SIR10-5220.pdf on 8/12/2015..
[44] *HighScore Plus*, version #4.0 (4.0.0) with PDF-2-release, ICDD, **2012**.

Received: May 11, 2015
Published Online: August 19, 2015

 © 2015 Wiley-VCH Verlag GmbH & Co. KGaA, Weinheim